Modeling the track geometry variability

G. Perrin, Christian Soize, Denis Duhamel, C. Fünfschilling

10th World Congress on Computational Mechanics
8-13 July 2012 • São Paulo • Brazil

MODELING THE TRACK GEOMETRY VARIABILITY.

G. Perrin[1,2,3], C. Soize[1], D. Duhamel[2], and C. Funfschilling[3]

[1] Université Paris-Est, Modélisation et Simulation Multi-Échelle (MSME UMR 8208 CNRS), 5 Bd. Descartes, 77454 Marne-la-Vallée, France. (guillaume.perrin@enpc.fr, christian.soize@univ-paris-est.fr)

[2] Université Paris-Est, Navier (UMR 8205 ENPC-IFSTTAR-CNRS), Ecole Nationale des Ponts et Chaussées, 6 et 8 Avenue Blaise Pascal, Cité Descartes, Champs sur Marne, 77455 Marne-la-Vallée, Cedex 2, France. (denis.duhamel@enpc.fr)

[3] SNCF, Innovation and Research Department, Immeuble Lumière, 40 avenue des Terroirs de France, 75611, Paris, Cedex 12, France. (christine.funfschilling@sncf.fr)

Abstract. *At its building, the theoretical new railway line is supposed to be made of perfect straight lines and curves. This track geometry is however gradually damaged and regularly subjected to maintenance operations. The analysis of these track irregularities is a key issue as the dynamic behaviour of the trains is mainly induced by the track geometry. In this context, this work is devoted to the development of a stochastic modeling of the track geometry and its identification with experimental measurements. Based on a spatial and statistical decomposition, this model allows the spatial and statistical variability and dependency of the track geometry to be taken into account. Moreover, it allows the generation of realistic track geometries that are representative of a whole railway network. These tracks can be used in any deterministic railway dynamic software to characterize the dynamic behavior of the train.*

Keywords: *Karhunen-Loève Reduction, Polynomial Chaos Expansion, Random fields, Railway Track Geometry.*

1. INTRODUCTION

High speed trains are currently meant to run faster and to carry heavier loads, while being less energy consuming and still respecting the security and comfort certification criteria. To face these new challenges, a better understanding of the interaction between the dynamic train behavior and the track geometry is of great concern.

The track-vehicle system being strongly non-linear, this dynamic interaction has therefore to be analyzed not only on a few track portions, but on most of the running conditions that, during its lifecycle, the train should be confronted to.

In reply to these expectations, the measurement train IRIS 320 has been running continuously since 2007 over the French railway network, measuring and recording the track geometry of the main national lines. Based on these experimental measurements, this paper develops a methodology to parameterize the physical properties as well as the variability of the track geometry. This modeling allows the numerical generation of track geometries that are physically realistic and statistically representative of a whole railway network. These tracks can be used as the input of a deterministic railway dynamic software to characterize the stochastic dynamic behavior of the train.

2. STOCHASTIC MODELING OF THE TRACK GEOMETRY

This section is devoted to the description of the track geometry modeling.

2.1. Track parametrization

Let $\mathcal{R}_0 = (O, \mathbf{X}_0, \mathbf{Y}_0, \mathbf{Z}_0)$ be the inertial reference frame. A railway track $\mathcal{T}$, of total length S^{tot}, is built up of two rails, which can be modeled in $\mathcal{R}_0$ as two parallel curves. Let $\boldsymbol{O}_{\text{NT}}$ be the mean position of the new track (without irregularities), which allows us to define the track curvilinear abscissa $0 \leq s \leq S^{\text{tot}}$, such that:

$$S^{\text{tot}} = \int_0^{S^{\text{tot}}} \sqrt{\|\boldsymbol{O}_{\text{NT}}(s)\|^2} ds. \tag{1}$$

As it has been presented in Section 1, a double scale parametrization is adopted in this paper to characterize the track geometry. Each rail position $\boldsymbol{R}_{\ell/r}$ (ℓ refers to the left rail whereas r refers to the right rail) is written as the sum of a mean position $\boldsymbol{M}_{\ell/r}$, which only depends on the curvilinear abscissia s, the track gauge E, the vertical and horizontal curvatures c_V and c_H and the track superelevation c_L, and a deviation towards this mean position $\boldsymbol{I}_{\ell/r}$, which only depends on the track irregularities vector $\boldsymbol{X}$:

$$\boldsymbol{R}_{\ell/r}(s) = \boldsymbol{M}_{\ell/r}(s) + \boldsymbol{I}_{\ell/r}(s). \tag{2}$$

The irregularities appearing during the track lifecycle are of four types (see Figure 1): lateral and vertical alignment irregularities X_1 and X_2 on the one hand, cant deficiencies X_3 and gauge irregularities X_4 on the other hand, such that:

$$\boldsymbol{M}_{\ell/r}(s) = \boldsymbol{O}_{\text{NT}}(s) \pm \frac{E}{2}\boldsymbol{N}(s), \tag{3}$$

$$\boldsymbol{I}_{\ell/r}(s) = \{X_2(s) \pm X_3(s)\}\,\boldsymbol{B}(s) + \{X_1(s) \pm X_4(s)\}\,\boldsymbol{N}(s), \tag{4}$$

where $(\boldsymbol{O}_{\text{NT}}(s), \mathbf{T}(s), \mathbf{N}(s), \mathbf{B}(s))$ is the Frenet frame. As the mean line description is chosen at the building of a new railway line for economical and political reasons, the present work focus on the description of the modeling of track irregularities vector $\boldsymbol{X} = (X_1, X_2, X_3, X_4)$.

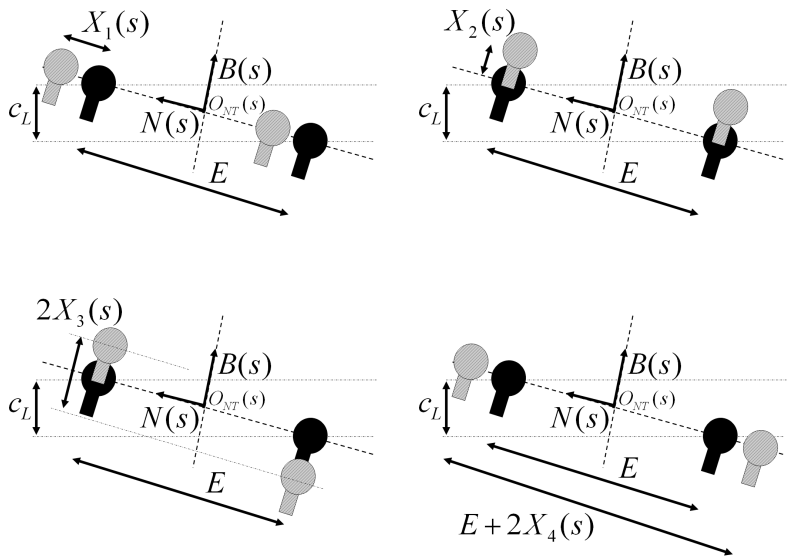

Figure 1. Parametrization of the track irregularities (for each rail, the mean position is represented in black, whereas the real position is in grey).

2.2. Theoretical frame

Let $(\Theta, \mathcal{C}, P)$ be a probability space. Let $\mathcal{H}$ be the space of all the second-order random variables defined on $(\Theta, \mathcal{C}, P)$ with values in $\mathbb{R}^4$, equipped with the inner product $\langle ., . \rangle$, such that for all $\boldsymbol{U}$ and $\boldsymbol{V}$ in $\mathcal{H}$,

$$\langle \boldsymbol{U}, \boldsymbol{V} \rangle = \int_{\Theta} \boldsymbol{U}^T(\theta) \boldsymbol{V}(\theta) dP(\theta) = E\left\{ \boldsymbol{U}^T \boldsymbol{V} \right\}, \tag{5}$$

where $E\{.\}$ is the mathematical expectation.

In this paper, a local-global approach is introduced, which implies that the whole track geometry $\mathcal{T}$ of length S^{tot} can be seen as the concatenation of ν^{exp} independent track portions of same length S, such that $S^{\text{tot}} = \nu^{\text{exp}} S$. The length S plays thus a key role in the modeling procedure and has to be carefully chosen.

Therefore, we consider in this paper that track irregularities vector $\boldsymbol{X}$ can be modelled by a second-order $\mathbb{R}^4$-valued stochastic process $\boldsymbol{X} = (X_1, X_2, X_3, X_4)$, indexed by $s \in \Omega = [0, S]$, whose realisations are almost surely in the Hilbert space $L^2(\Omega, \mathbb{R}^4)$ equipped with the inner product $(., .)$:

$$(\boldsymbol{u}, \boldsymbol{v}) = \int_{\Omega} \boldsymbol{u}^T(s) \boldsymbol{v}(s) ds, \quad \forall \boldsymbol{u}, \boldsymbol{v} \in L^2(\Omega, \mathbb{R}^4). \tag{6}$$

It is assumed that $\boldsymbol{X}$ is mean-square continuous, and that its mean value $E\{\boldsymbol{X}(s)\}$ is zero. From the experimental measurements, ν^{exp} track portions $\left\{ \boldsymbol{x}^1, \cdots, \boldsymbol{x}^{\nu^{\text{exp}}} \right\}$ of same length S are extracted, which defines the maximum available information for the stochastic modeling. It has to be noticed that gathering all the irregularities in the same vector, $\boldsymbol{X}$, and adopting a vectorial approach certifies that the inner dependencies between different irregularity fields are accurately taken into account.

2.3. Truncated Karhunen-Loève expansion

For all $(s, s') \in \Omega^2$, let $[R_{\boldsymbol{XX}}(s, s')] = E\left\{\boldsymbol{X}(s)\boldsymbol{X}^T(s')\right\}$ be the autocorrelation matrix of random field $\boldsymbol{X}$. Under the asumptions above, $[R_{\boldsymbol{XX}}]$ is continuous on $\Omega \times \Omega$, positive-definite and can be written as:

$$[R_{\boldsymbol{XX}}(s, s')] = \sum_{k\geq 1} \lambda_k \boldsymbol{u}^k(s)\ {\boldsymbol{u}^k}^T(s'), \tag{7}$$

where $\left(\lambda_k, \boldsymbol{u}^k\right)$ is an orthonormal basis of $L^2(\Omega, \mathbb{R}^4)$ solution of the Fredholm equation (see [1] and [2] for further details). The values λ_k are non-negative, and can be arranged in decreasing order: $\lambda_1 \geq \lambda_2 \geq \cdots \to 0$. The truncated Karhunen-Loève expansion of the stochastic process $\boldsymbol{X}$ is then:

$$\boldsymbol{X}(s) \approx \widehat{\boldsymbol{X}}(s) = \sum_{k=1}^{N_x} \sqrt{\lambda_k}\boldsymbol{u}^k(s)\eta_k, \tag{8}$$

$$\eta_k = \frac{1}{\sqrt{\lambda_k}}\left(\boldsymbol{X}, \boldsymbol{u}^k\right), \tag{9}$$

where N_x is related to a chosen value of the normalized mean-square error:

$$\epsilon^2 = E\left\{\left(\boldsymbol{X} - \widehat{\boldsymbol{X}}, \boldsymbol{X} - \widehat{\boldsymbol{X}}\right)\right\} = \frac{\sum_{k>N_x}\lambda_k}{E\left\{(\boldsymbol{X}, \boldsymbol{X})\right\}}. \tag{10}$$

Equations (7) and (8) imply that, for $1 \leq k, \ell \leq N_x$:

$$E\left\{\eta_k\eta_\ell\right\} = \delta_{k\ell.} \tag{11}$$

For a given value of N_x, it can be shown that projection basis $\left\{\boldsymbol{u}^k,\ 1 \leq k \leq N_x\right\}$ is optimal in the sense that it minimizes error ϵ^2 among the set of all the N_x-elements basis. Moreover, thanks to this expansion, spatial and statistical correlations are clearly separated. Whereas $\left\{\boldsymbol{u}^k,\ 1 \leq k \leq N_x\right\}$ emphasizes the predominant track irregularity spatial shapes, $\boldsymbol{\eta} = (\eta_1, \cdots, \eta_{N_x})$ characterizes the statistical variability of $\boldsymbol{X}$. In order to fully describe track irregularity vector $\boldsymbol{X}$, the statistical content of $\boldsymbol{\eta}$, and more specially its joint probability density function (PDF) $p_{\boldsymbol{\eta}}$ has to be focused on.

2.4. Polynomial Chaos Expansion

From the $\nu^{\exp}$ track portions $\left\{\boldsymbol{x}^1, \cdots, \boldsymbol{x}^{\nu^{\exp}}\right\}$, $\nu^{\exp}$ independent realizations, that we call $\{\boldsymbol{\eta}(\theta_1), \cdots, \boldsymbol{\eta}(\theta_{\nu^{\exp}})\}$, of $\boldsymbol{\eta}$ can be deduced as:

$$\forall\ 1 \leq k \leq N_x,\ 1 \leq i \leq \nu^{\exp},\ \eta_k(\theta_i) = \frac{1}{\sqrt{\lambda_k}}\left(\boldsymbol{x}^i, \boldsymbol{u}^k\right). \tag{12}$$

The fact that $E\left\{\boldsymbol{X}(s)\right\} = \boldsymbol{0}$ and Eq. (11) imply two constraints on joint PDF $p_{\boldsymbol{\eta}}$ of $\boldsymbol{\eta}$:

$$E\left\{\boldsymbol{\eta}\right\} = \boldsymbol{0},\ \ E\left\{\boldsymbol{\eta}\boldsymbol{\eta}^T\right\} = [I_{N_x}], \tag{13}$$

where $[I_{N_x}]$ is the N_x-dimension identity matrix. Therefore, random variables η_1,...,η_{N_x} are statistically orthogonal, but are generally not independent. Two kinds of methods can be used

to build such a PDF $p_{\boldsymbol{\eta}}$: the direct and the indirect methods. The indirect methods allow the construction of the PDF $p_{\boldsymbol{\eta}}$ of the considered random vector $\boldsymbol{\eta}$ from a transformation $\mathbb{H}$ of a known PDF $p_{\boldsymbol{\xi}}$ of a random vector $\boldsymbol{\xi} = \left(\xi_1, ..., \xi_{N_g}\right)$ of given dimension $N_g \leq N_\eta$:

$$\boldsymbol{\eta} = \boldsymbol{t}\left(\boldsymbol{\xi}\right), \;\; p_{\boldsymbol{\eta}} = \mathbb{T}\left(p_{\boldsymbol{\xi}}\right). \tag{14}$$

The construction of the transformation $\boldsymbol{t}$ is thus the key point of these indirect methods. In this context, the isoprobabilist transformations such as the Nataf transformation (see [3]) or the Rosenblatt transformation (see [4]) have allowed the development of interesting results in the second part of the twentieth century but are still limited to very small dimension cases. Nowadays, the most popular indirect methods are the polynomial chaos expansion (PCE) methods, which have been first introduced by Wiener [5] for stochastic processes, and generalized by Ghanem and Spanos ([6] [7]). The PCE is based on a direct projection of the random vector $\boldsymbol{\eta}$ on a chosen orthonormal basis $\mathcal{B}_{orth} = \left\{\psi_{\boldsymbol{\alpha}}(\boldsymbol{\xi}), \boldsymbol{\alpha} \in \mathbb{N}^{N_g}\right\}$ of its probability space, such that:

$$\boldsymbol{\xi} \mapsto \psi_{\boldsymbol{\alpha}}(\boldsymbol{\xi}) = X_{\alpha_1}(\xi_1) \otimes ... \otimes X_{\alpha_{N_g}}(\xi_{N_g}), \tag{15}$$

where $x \mapsto X_{\alpha_\ell}(x)$ is the normalized polynomial basis of degree α_ℓ associated to the PDF p_{ξ_ℓ} of the random variable ξ_ℓ, and $\boldsymbol{\alpha}$ is the multi-index of the multidimensional polynomial basis element $\psi_{\boldsymbol{\alpha}}(\boldsymbol{\xi})$.

In practical terms, the PCE projection has to be truncated. Two truncation parameters are usually introduced in this prospect: we define N_g as the maximal size of PCE germ $\boldsymbol{\xi}$ and p as the maximal polynomial order of the elements of the orthogonal basis $\mathcal{B}_{orth}$, which allows us to approximate $\boldsymbol{\eta}$ by its truncated PCE expansion $\boldsymbol{\eta}^{\text{chaos}}(N_g, p)$:

$$\boldsymbol{\eta} \approx \boldsymbol{\eta}^{\text{chaos}}(N_g, p) = E\left\{\boldsymbol{\eta}\right\} + \sum_{\boldsymbol{\alpha} \in \boldsymbol{\mathcal{A}}_p} \boldsymbol{y}^{(\boldsymbol{\alpha})} \psi_{\boldsymbol{\alpha}}(\boldsymbol{\xi}) = E\left\{\boldsymbol{\eta}\right\} + [y]\boldsymbol{\Psi}(\boldsymbol{\xi}), \tag{16}$$

$$\boldsymbol{\mathcal{A}}_p = \left\{ \boldsymbol{\alpha} = \left(\alpha_1, ..., \alpha_{N_g}\right) \mid 0 < \; |\boldsymbol{\alpha}| = \sum_{i=1}^{N_g} \alpha_i \leq p \right\}, \tag{17}$$

where $N = (N_g + p)!/(N_g! + p!) - 1$ is the dimension of $\boldsymbol{\mathcal{A}}_p$. The values of N_g and p have to be identified according to an analysis of convergence. It can be noticed that the conditions, defined by Eq. (13) can be rewritten as:

$$\boldsymbol{\eta}^{\text{chaos}}(N_g, p) = [y]\boldsymbol{\Psi}(\boldsymbol{\xi}), \;\; [y] \in \tilde{\mathcal{O}} = \left\{ [b] \in \mathbb{M}_{N_x, N}(\mathbb{R}) \mid [b][b]^T = [I_{N_x}] \right\}. \tag{18}$$

Based on the maximum likelihood principle, and the ν^{exp} independant realisations $\{\boldsymbol{\eta}(\theta_i), \; 1 \leq i \leq \nu^{\text{exp}}\}$ of $\boldsymbol{\eta}$, a good approach to identify PCE coefficient matrix $[y]$ is to search it as the result of the maximization problem:

$$[y] = \arg\max_{[y] \in \tilde{\mathcal{O}}} \mathcal{L}\left([y]\right), \tag{19}$$

where $\mathcal{L}$ is the evaluation of the log-likelihood function of $\boldsymbol{\eta}^{\text{chaos}}(N_g, p)$ at the experimental points $\{\boldsymbol{\eta}(\theta_i),\ 1 \leq i \leq \nu^{\text{exp}}\}$. As $\mathcal{L}$ is non concave, random maximization algorithms have to be used to compute numerically $[y]$. The optimization problem, defined by Eq. (19) is now supposed to be solved with the advanced algorithms described in [8] and [9].

2.5. Generation of a whole track geometry

Once projection basis $\left\{\boldsymbol{u}^k,\ 1 \leq k \leq N_x\right\}$ and PCE coefficient matrix $[y]$ have been identified, the irregularity vector $\boldsymbol{X}$ can be expressed as:

$$\forall\ s \in \Omega,\ \boldsymbol{X}(s) \approx \widetilde{\boldsymbol{X}}\,(s, \boldsymbol{\xi}) = \sum_{k=1}^{N_x} \sum_{j=1}^{N} \sqrt{\lambda_k}\boldsymbol{u}^k [y]_{kj} \Psi_j(\boldsymbol{\xi}). \tag{20}$$

The elements $\left\{\boldsymbol{u}^k,\ 1 \leq k \leq N_x\right\}$ and matrix $[y]$ are both deterministic, whereas $\boldsymbol{\xi}$ is a random vector whose distribution is known. Hence, each realization of $\boldsymbol{\xi}$ leads us to the computation of a realistic and representative track geometry of length S. Thanks to the local-global approach, described in Section 2.2, a whole track geometry of length $S^{\text{tot}} = N_{\mathcal{T}} S$ ($N_{\mathcal{T}}$ can be smaller or greater than ν^{exp}), $\left\{\boldsymbol{X}^{\text{tot}}(s),\ s \in [0, S^{\text{tot}}]\right\}$, can therefore be constructed from $N_{\mathcal{T}}$ copies $\widetilde{\boldsymbol{X}}(\boldsymbol{\xi}^{(1)}), \cdots, \widetilde{\boldsymbol{X}}(\boldsymbol{\xi}^{(N_{\mathcal{T}})})$ of track irregularity stochastic process $\left\{\widetilde{\boldsymbol{X}}(s, \boldsymbol{\xi}),\ s \in [0, S]\right\}$, such that:

$$\forall\, 1 \leq n \leq N_{\mathcal{T}},\ \forall\ s \in [S\,(n-1)\,, Sn],\ \ \boldsymbol{X}^{\text{tot}}(s) = \widetilde{\boldsymbol{X}}(s, \boldsymbol{\xi}^{(n)}). \tag{21}$$

However, for each particular realization $\boldsymbol{X}^{\text{tot}}(\Theta)$ of $\boldsymbol{X}^{\text{tot}}$, a particular attention has to be paid at the interface between the different realizations $\widetilde{\boldsymbol{X}}(\boldsymbol{\xi}^{(1)}(\Theta)), \cdots, \widetilde{\boldsymbol{X}}(\boldsymbol{\xi}^{(N_{\mathcal{T}})}(\Theta))$. Indeed, these jonctions have to guarantee the continuity of the track irregularity vector and at least the continuity of its first and second order spatial derivatives $\dot{\boldsymbol{X}}^{\text{tot}}$ and $\ddot{\boldsymbol{X}}^{\text{tot}}$, but also the continuity of their statistical moments to avoid an artificial perturbation for the train dynamics. This continuity at the jonction between track portions of length S is therefore guaranteed by drawing $\boldsymbol{\xi}^{(1)}(\Theta)$ according to its chosen distribution, $P_{\boldsymbol{\xi}}$, and for all $2 \leq n \leq N_{\mathcal{T}}$, by drawing realizations $\boldsymbol{\xi}^{(n)}(\Theta)$ according to the conditional probability

$$\begin{aligned}
&P_{\boldsymbol{\xi}}^{C}\left(\widetilde{\boldsymbol{X}}(S, \boldsymbol{\xi}^{(n-1)}(\Theta)), \dot{\widetilde{\boldsymbol{X}}}(S, \boldsymbol{\xi}^{(n-1)}(\Theta)), \ddot{\widetilde{\boldsymbol{X}}}(S, \boldsymbol{\xi}^{(n-1)}(\Theta))\right) \\
&= P\left(\boldsymbol{\xi}^{(n)} \sim P_{\boldsymbol{\xi}}\ \mid\ \widetilde{\boldsymbol{X}}(0, \boldsymbol{\xi}^{(n)}(\Theta)) = \widetilde{\boldsymbol{X}}(S, \boldsymbol{\xi}^{(n-1)}(\Theta)),\ \dot{\widetilde{\boldsymbol{X}}}(0, \boldsymbol{\xi}^{(n)}(\Theta)) = \dot{\widetilde{\boldsymbol{X}}}(S, \boldsymbol{\xi}^{(n-1)}(\Theta)),\right. \\
&\left.\ddot{\widetilde{\boldsymbol{X}}}(0, \boldsymbol{\xi}^{(n)}(\Theta)) = \ddot{\widetilde{\boldsymbol{X}}}(S, \boldsymbol{\xi}^{(n-1)}(\Theta))\right).
\end{aligned} \tag{22}$$

Therefore, the proposed stochastic modeling allows us to generate realistic track geometries of length $S^{\text{tot}} = N_{\mathcal{T}} S$ that are representative of the whole considered network.

3. APPLICATION

In this section, the previously described methodology is applied to the characterization of the track geometry variability of the French high speed line between Paris and Marseille.

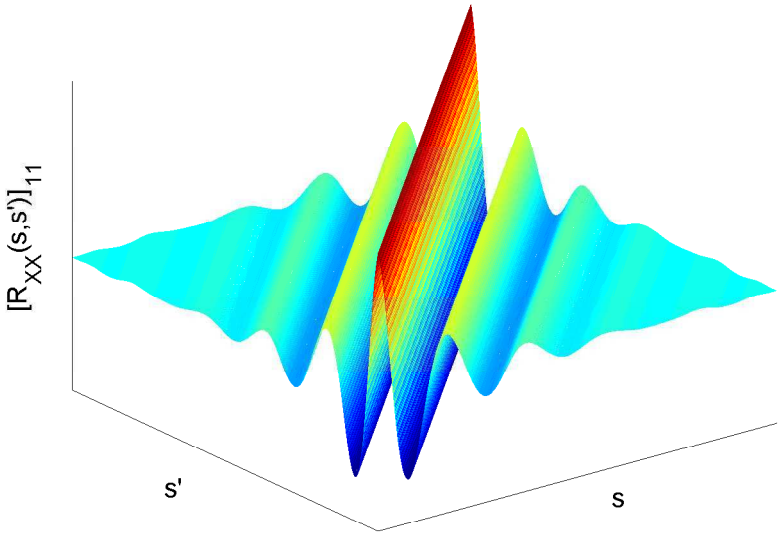

Figure 2. Representation of $(s, s') \mapsto [R_{\boldsymbol{XX}}(s, s')]_{11}$

This study being confidential, only normalized values are presented.

3.1. Evaluation of the autocorrelation matrix

For this study, $\nu^{\text{exp}} = 1850$ track irregularity measurements, $\{\boldsymbol{x}^i,\ 1 \leq i \leq \nu^{\text{exp}}\}$, of same length S have been gathered, which allows us to estimate the autocorrelation matrix $[R_{\boldsymbol{XX}}(s, s')]$ as:

$$[R_{\boldsymbol{XX}}(s, s')] \approx \frac{1}{\nu^{\text{exp}}} \sum_{i=1}^{\nu^{\text{exp}}} \boldsymbol{x}^i(s)\boldsymbol{x}^i(s')^T. \tag{23}$$

As an illustration, matrix $[R_{\boldsymbol{XX}}(s, s')]_{11}$ is represented in Figure 2.

3.2. Karhunen-Loève expansion

The solutions $(\boldsymbol{u}, \lambda)$ of the Fredholm equation were then computed thanks to a Finite Element approach. Given acceptable values of truncation for the mean-square error ϵ^2 (10% in our study) of Eq. (10) (for which evolution is represented in Figure 3), truncation parameter N_x of Eq. (8) is identified:

$$\epsilon^2 = 10\% \leftrightarrow N_x = 452. \tag{24}$$

From Eq. (12), the ν^{exp} realisations $\{\boldsymbol{\eta}(\theta_i),\ 1 \leq i \leq \nu^{\text{exp}}\}$ of $\boldsymbol{\eta}$ are computed. In Figure 4, the PDF of η_1, η_2 and η_3 are represented and compared to the normal distribution.

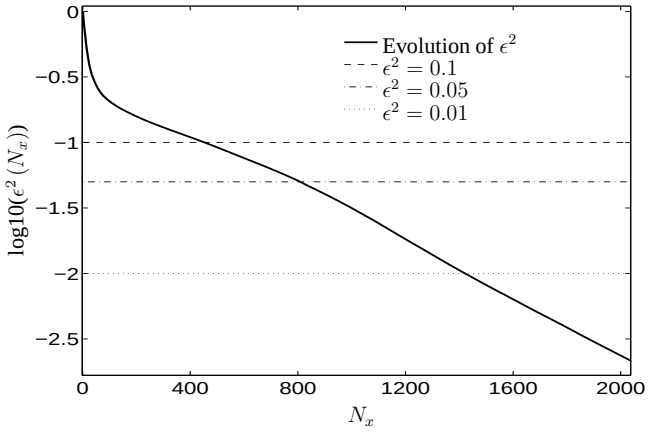

Figure 3. Representation of the Mean-Square Error ϵ^2 with respect to truncation parameter N_x

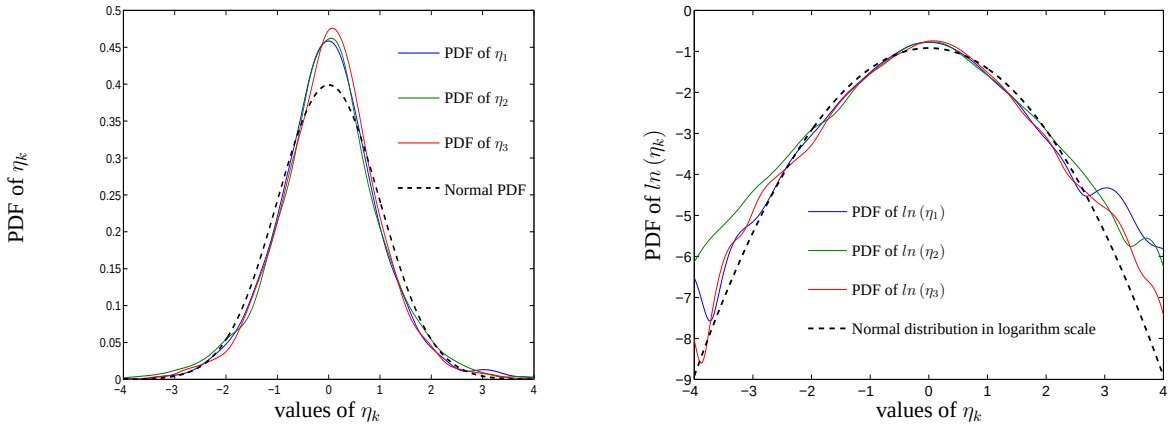

Figure 4. Representation of three marginal PDFs of $\boldsymbol{\eta}$.

It can therefore be noticed that the marginal distributions of $\boldsymbol{\eta}$ are non-Gaussian: the random process $\boldsymbol{X}$ is thus non Gaussian. Its joint PDF has therefore to be properly characterized.

3.3. Polynomial Chaos Expansion

As presented in the former section, $\boldsymbol{\eta}$ is projected on a known truncated polynomial basis, which is expressed with respect to two truncation parameters N_g and p:

$$\boldsymbol{\eta} \approx \boldsymbol{\eta}^{\text{chaos}}(N_g, p) = [y]\boldsymbol{\Psi}\left(\xi_1, ..., \xi_{N_g}\right), \tag{25}$$

where $[y]$ is solution of Eq. (19).

The values of N_g et p have to be identified according to a convergence analysis. In this prospect, the following L^1-log error function err_k is introduced:

$$\forall 1 \leq k \leq N_x, \quad err_k(N_g, p) = \int_{BI_k} |log_{10}\left(p_{\eta_k}(x)\right) - log_{10}\left(p_{\eta_k^{\text{chaos}}}(x)\right)| dx, \tag{26}$$

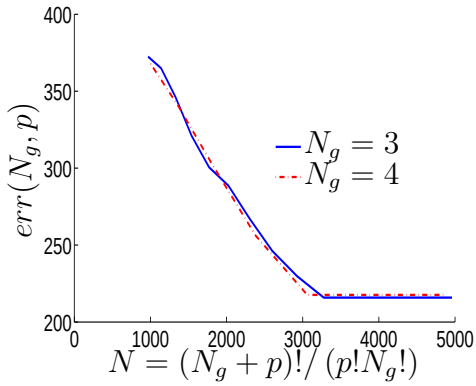

Figure 5. Convergence analysis for the PCE expansion of $\boldsymbol{\eta}$.

where:

- BI_k is a bounded domain which has to be adapted to the values of η_k;
- p_{η_k} and $p_{\eta_k^{\text{chaos}}}$ are the PDFs of the elements η_k and $\eta_k^{\text{chaos}}(N_g, p)$ of random vectors $\boldsymbol{\eta}$ and $\boldsymbol{\eta}_k^{\text{chaos}}(N_g, p)$ respectively.

The final values of N_g and p are then deduced from the convergence of the multidimensional error function $err(N_g, p)$, which is expressed with respect to the former unidimensional L^1-log error functions:

$$(N_g, p) = \arg \min_{N_g^*, p^*} err(N_g^*, p^*), \tag{27}$$

$$err(N_g, p) = \sum_{k=1}^{N_x} err_k(N_g, p). \tag{28}$$

Figure 5 shows the convergence of this error. Hence, the truncation parameters N_g and p are chosen respectively equal to 3 and 26, such that the size of the PCE basis, N, is equal to 3654.

3.4. Generation of representative track geometries

According to Section 2.5, once deterministic matrix $[y]$ has been computed, one can generate track geometries that are realistic and representative of the high speed line between Paris and Marseille. As an illustrution, a particular extract of length S of complete track geometry is represented in Figure 6. This graph has been centered at abscissa $s = 3S/2$, that is to say at the jonction between the two first track portions. In order to allow a better visualization of the results, the four components of the track irregularity vector have been represented in the same graph, but their values have been shifted.

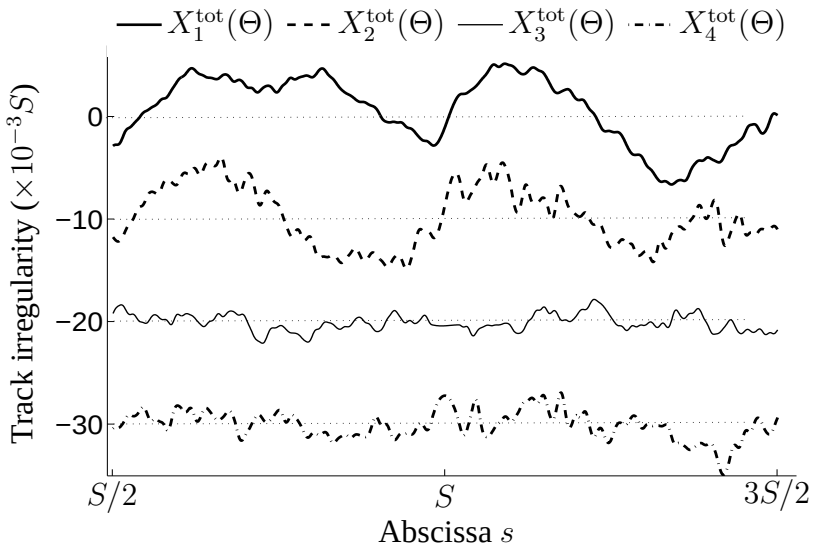

Figure 6. Extract of a simulated track geometry.

4. CONCLUSIONS

At a time when the numerical power and the mechanical simulation algorithms precision keep increasing, the introduction of the simulation in the railway maintenance and certification would represent an important progress. The numerical characterization of the track geometry is therefore bound to play a key role in this evolution.

From a sample of track measurements, a complete methodology to generate realistic and representative track geometries has been described in this paper.

Coupled with any railway software without requiring an access to the sources codes, these track geometries makes up a very useful database to analyze the complex link between the train dynamics and the physical and statistical properties of the track geometry.

References

[1] O.P. Le Maître and O.M. Knio. *Spectral Methods for Uncertainty Quantification*. Springer, 2010.

[2] G. Perrin, C. Soize, D. Duhamel, and C. Funfschilling. Track irregularities stochastic modeling. *Probabilistic Engineering Mechanics*, (submitted February 2012).

[3] A. Nataf. Détermination des distributions de probabilité dont les marges sont données. *Comptes Rendus de l'Académie des Sciences*, 225:42–43, 1986.

[4] M. Rosenblatt. Remarks on a multivariate transformation. *Annals of Mathematical Statistics*, 23:470–472, 1952.

[5] N. Wiener. The homogeneous chaos. *American Journal of Mathematics*, 60:897–936, 1938.

[6] R. Ghanem and P.D. Spanos. Polynomial chaos in stochastic finite elements. *Journal of Applied Mechanics*, Transactions of teh ASME 57:197–202, 1990.

[7] R. Ghanem and P. D. Spanos. *Stochastic Finite Elements: A Spectral Approach, rev. ed.* Dover Publications, New York, 2003.

[8] C. Soize. Identification of high-dimension polynomial chaos expansions with random coefficients for non-gausian tensor-valued random fields using partial and limited experimental data. *Computer Methods in Applied Mechanics and Engineering*, 199:2150–2164, 2010.

[9] G. Perrin, C. Soize, D. Duhamel, and C. Funfschilling. Identification of polynomial chaos representations in high dimension from a set of realisations. *Society for Industrial and Applied Mathematics - Journal on Scientific Computing*, (accepted May 2012).